The Astrophysical Journal, 631:856–867, 2005 October 1

PROBING THE LOCAL GROUP MEDIUM TOWARD MARKARIAN 421 WITH *CHANDRA* AND THE *FAR ULTRAVIOLET SPECTROSCOPIC EXPLORER*

Rik J. Williams,[1] Smita Mathur,[1] Fabrizio Nicastro,[2,3] Martin Elvis,[2] Jeremy J. Drake,[2] Taotao Fang,[4,5] Fabrizio Fiore,[6] Yair Krongold,[2,3] Q. Daniel Wang,[7] and Yangsen Yao[7]

Received 2004 December 16; accepted 2005 May 17

ABSTRACT

We report the detection of highly ionized gas at $z \sim 0$ seen in resonant UV and X-ray absorption lines toward the $z = 0.03$ blazar Mrk 421. A total of 13 X-ray and three UV lines were measured (or upper limits derived), including three lines in the O VII K series and Kα transitions from neon, carbon, and nitrogen. From the three O VII lines we derive a 2 σ Doppler parameter constraint of 24 km s^{-1} $< b <$ 55 km s^{-1}. The *FUSE* spectrum shows strong Galactic low-velocity O VI λ1032 absorption and a possible weak O VI high-velocity component (HVC). The Doppler parameter of the low-velocity O VI measured with *FUSE* is $\sim$3 σ higher than that derived from the O VII line ratios, indicating that the O VII and Galactic O VI arise in different phases. This velocity dispersion along with limits on the gas temperature and density from the X-ray line ratios (assuming a single phase with collisional ionization equilibrium plus photoionization) are all consistent with an extragalactic absorber. However, the O VII Doppler parameter is inconsistent with the high temperature required to produce the observed O VI$_{\rm HVC}$/O VII ratio, implying that the HVC is probably not related to the O VII. In addition, the O VI$_{\rm K\alpha}$ line detected by *Chandra* implies a column density $\sim$4 times higher than the λ1032 absorption. Although an extragalactic absorber is fully consistent with the measured column density ratios, a Galactic origin cannot be ruled out given the uncertainties in the available data.

Subject headings: Galaxy: halo — intergalactic medium — quasars: absorption lines

1. INTRODUCTION

At both low and high redshifts, the intergalactic medium (IGM) is thought to be the dominant reservoir of baryonic matter in the universe. Essentially all of the baryons at $z \sim 2$ are accounted for in the "forest" of H I Lyα absorption lines seen against background quasars (Weinberg et al. 1997). In the local universe, numerical simulations predict that most of the IGM is in the form of a shock-heated "warm-hot IGM" (WHIM) with $T \sim 10^5$–10^7 K and densities $n_{\rm H} \sim 10^{-6}$ to 10^{-5} cm^{-3} (Cen & Ostriker 1999; Davé et al. 2001). Hydrogen is mostly ionized at these temperatures, rendering it difficult or impossible to detect. However, H-, He-, and Li-like ions of heavier elements can exist under these conditions, producing a "forest" of low-z intervening UV/X-ray absorption lines in quasar spectra (Hellsten et al. 1998; Perna & Loeb 1998). In particular, O VI, O VII, and O VIII are expected to produce the strongest lines (depending on the temperature and ionizing background).

The required sensitivity to detect such absorption systems is now available with the advent of such facilities as the *Chandra X-Ray Observatory*, *XMM-Newton*, *Hubble Space Telescope*, and the *Far Ultraviolet Spectroscopic Explorer* (*FUSE*). High signal-to-noise ratio (S/N) observations along four lines of sight reveal such intervening absorption systems with temperatures and densities consistent with the WHIM (Nicastro et al. 2005a, 2005b, 2005c; Mathur et al. 2003; Fang et al. 2002; T. Fang et al. 2005, in preparation). In addition, the total baryonic mass density in these detected filaments is consistent with the 2.5% $\pm$ 0.4% deficiency between cosmic microwave background measurements (Bennett et al. 2003) and previous density measurements of stars and gas (see also Nicastro et al. 2005b and references therein).

Since most galaxies are expected to trace the same cosmic overdensities as the web of IGM filaments, it would be no surprise if the Galaxy itself resided in such a filament. Indeed, X-ray spectra of several quasars show likely $z = 0$ O VII absorption, e.g., PKS 2155−304 (Nicastro et al. 2002), 3C 273 (Fang et al. 2003), and Mrk 279 (R. J. Williams et al. 2005, in preparation). The upper limit found for O VII emission implies that O VII *absorption* systems most likely arise in an extragalactic medium (Rasmussen et al. 2003); however, the analysis is complicated by $z = 0$ O VI absorption observed with *FUSE* along many quasar lines of sight (Wakker et al. 2003). The strongest O VI absorption component, typically within $v_{\rm LSR} = \pm 100$ km s^{-1} (hereafter denoted O VI$_{\rm LV}$), is due to gas in the halo and thick disk of the Galaxy (Savage et al. 2003). Of the 102 sight lines studied, 84 show at least one additional O VI high-velocity component (HVC), typically weaker than the O VI$_{\rm LV}$.

The origin and location of the O VI HVCs are controversial: while some may be spatially and kinematically associated with known Galactic structure (such as the Magellanic Stream and H I high-velocity clouds, although this association is in many cases uncertain), others appear to be completely isolated. Sembach (2003) summarizes the evidence in favor of a Galactic origin for the O VI HVCs. In such a scenario, the absorption could arise at the interface between infalling cooler gas clouds and very hot ($T > 10^6$ K) gas in an extended Galactic corona. The observed gas stripping and orbital deflection of the Magellanic Clouds

[1] Department of Astronomy, Ohio State University, 140 West 18th Avenue, Columbus, OH 43210; williams@astronomy.ohio-state.edu, smita@astronomy.ohio-state.edu.
[2] Harvard-Smithsonian Center for Astrophysics, 60 Garden Street, Cambridge, MA 02138; fnicastro@cfa.harvard.edu.
[3] Instituto de Astronomía Universidad Autónomica de México, Apartado Postal 70-264, Ciudad Universitaria, Mexico, D.F., CP 04510, Mexico.
[4] Department of Astronomy, University of California, 601 Campbell Hall, Berkeley, CA 94720.
[5] Chandra Fellow.
[6] Osservatorio Astronomico di Roma, Sede di Monteporzio Catone, Via di Frascati, 33, Rome I-00040, Italy.
[7] Department of Astronomy, University of Massachusetts, 710 North Pleasant Street, Amherst, MA 01003.

also lend credence to such a low-density corona. Furthermore, lower ionization species such as Si IV and C IV are seen toward some sight lines. Thus, there is some evidence for a collisionally ionized, high-density Galactic medium.

On the other hand, there is also evidence that the isolated O VI HVCs trace the Local Group medium and thus are associated with the $z = 0$ O VII and O VIII X-ray absorption. The most compelling evidence for this interpretation is the velocity segregation of the O VI HVCs: Nicastro et al. (2003) report that the mean velocity vector of the O VI HVCs is highest in the local standard of rest and lowest in the Local Group rest frame, implying an extragalactic, Local Group origin. The presence of lower ionization lines does not rule out a WHIM origin for the O VI HVCs since the medium is likely inhomogeneous and may thus consist of phases of different temperatures and densities (such as the intervening WHIM absorbers found by Danforth & Shull 2005). Furthermore, isolated high-velocity O VI (which is not associated with O I and other low-ionization lines) has not been detected toward high-latitude Galactic sources out to 10 kpc (Danforth et al. 2002; Howk et al. 2003; Zsargó et al. 2003). The low-ionization line profiles often differ substantially from the O VI HVCs, implying that they may arise in different components (Collins et al. 2005).

The key to understanding the O VI absorption is higher quality X-ray data, since the O VII and O VIII along high-latitude quasar sight lines are the most likely to trace the WHIM (i.e., least subject to possible contamination by hot Galactic gas). X-ray measurements by themselves provide great insight into the properties of the local WHIM, including its mass and extent, thereby yielding valuable constraints for models of galaxy formation and the Local Group (e.g., Kravtsov et al. 2002). However, knowing whether the O VI HVCs are also associated with the WHIM provides even stronger diagnostics. Unfortunately, existing X-ray data have not been of sufficiently high quality to resolve this ambiguity: even at large column densities ($N_i \sim 10^{15}$ cm^{-2}), X-ray lines are quite weak, and several thousand counts per resolution element in a typical *Chandra* grating spectrum are required to accurately measure these lines.

Through our program of observing nearby blazars in outburst phases, we have obtained high-quality *Chandra* and *FUSE* spectra of Mrk 421, sufficient to study in detail the local WHIM (and Galactic halo/thick disk) absorption. Here we report on these observations and the inferred properties of the local absorption.

2. OBSERVATIONS AND DATA PREPARATION

2.1. *Chandra*

A full description of the *Chandra* observations, data reduction, and continuum fitting can be found in Nicastro et al. (2005b); a brief summary follows. Mrk 421 was observed during two exceptionally high outburst phases for 100 ks each as part of our *Chandra* AO4 observing program: one at $f_{0.5-2\,\mathrm{keV}} = 1.2 \times 10^{-9}$ ergs s^{-1} cm^{-2} with the Low Energy Transmission Grating (LETG) combined with the Advanced CCD Imaging Spectrometer (ACIS-S; Garmire et al. 2003) array, and another at $f_{0.5-2\,\mathrm{keV}} = 0.8 \times 10^{-9}$ ergs s^{-1} cm^{-2} with the High Resolution Camera (HRC-S; Murray & Chappell 1986) array and LETG. Each of these observations contains ~2500 counts per resolution element at 21.6 Å. In addition, another short observation of Mrk 421 was taken with HRC/LETG (2004 May 29), providing another 170 counts per resolution element. These three spectra were combined over the 10–60 Å range to improve the S/N (S/N ~ 55 at 21 Å with 0.0125 Å binning). The final co-added spectrum of Mrk 421 is one of the best ever taken with *Chandra*: it contains over 10^6 total counts with ~6000 counts per resolution element at 21.6 Å, providing a 3 σ detection threshold of $W_\lambda \sim 2$ mÅ ($N_{\mathrm{O\,VII}} = 8 \times 10^{14}$ cm^{-2} for an unsaturated line).

Effective area files (ARFs) for each observation were built using CIAO[8] version 3.0.2 and CALDB[9] version 2.2.6. Those pertaining to the ACIS/LETG observations were corrected for the ACIS quantum efficiency degradation[10] (Marshall et al. 2004). For the HRC/LETG observations, the standard ARFs were used. Each ARF was then convolved with the relevant standard redistribution matrix file (RMF), and the convolved RMFs were weighted by exposure time, rebinned to the same energy scale, and averaged to provide a response file for the co-added spectrum.

Using the CIAO fitting package Sherpa,[11] we initially modeled the continuum of Mrk 421 as a simple power law and a Galactic absorbing column density of $N_{\mathrm{H}} = 1.4 \times 10^{20}$ cm^{-2} (Dickey & Lockman 1990), excluding the 48–57 Å HRC chip gap region. Metal abundances for the Galactic gas were then artificially adjusted to provide a better fit around the O I and C I K edges near 23 and 43 Å, respectively. This is *not* intended to represent actual changes to the absorber composition, but rather to correct uncertainties in the instrument calibration. These adjustments affect the continuum mostly near the carbon, oxygen, and neon edges, but individual narrow absorption lines are unaffected. After this fit there were still some systematic uncertainties in the best-fit continuum model; these were corrected with broad (FWHM = 0.15–5 Å) Gaussian emission and absorption components until the modeled continuum appeared to match the data upon inspection. Indeed, the residuals of the spectrum to the final continuum model have a nearly Gaussian distribution, with a negative tail indicating the presence of narrow absorption lines (see Nicastro et al. 2005b, Fig. 8).

2.2. *FUSE*

Mrk 421 was also observed with *FUSE* as part of our Director's Discretionary Time observing program on 2003 January 19–21 for a total of 62.8 ks. An additional 21.8 ks observation from 2000 December 1 was also available in the archive. We used the time-tagged, calibrated data from only the LiF1A detector, since inclusion of the LiF2B data provides a small (~20%) increase in S/N but degrades the overall spectral resolution.[12] These two observing programs consist of four observations, which in turn contain a total of 29 individual exposures. The wavelength scales of each observation's constituent exposures were cross-correlated and shifted (typically by 1–2 pixels) to account for slight uncertainties in the wavelength calibration. The exposures for each observation were checked for consistency and co-added, weighted by exposure time. The resulting four spectra were then cross-correlated against each other, co-added (with a ~10% downward shift in flux applied to the 2000 observation due to source variability), and binned by 5 pixels (0.034 Å, or one-half of the nominal 20 km s^{-1} resolution), providing an S/N of 17 near 1032 Å.

To check the absolute wavelength calibration, we followed the method of Wakker et al. (2003), using their four-component fit to

[8] Available at http://cxc.harvard.edu/ciao.
[9] Available at http://cxc.harvard.edu/caldb.
[10] See also http://cxc.harvard.edu/ciao/why/acisqedeg.html.
[11] Available at http://cxc.harvard.edu/sherpa.
[12] See the *FUSE* Data Analysis Cookbook ver. 1.0, http://fuse.pha.jhu.edu/analysis/analysis.html.

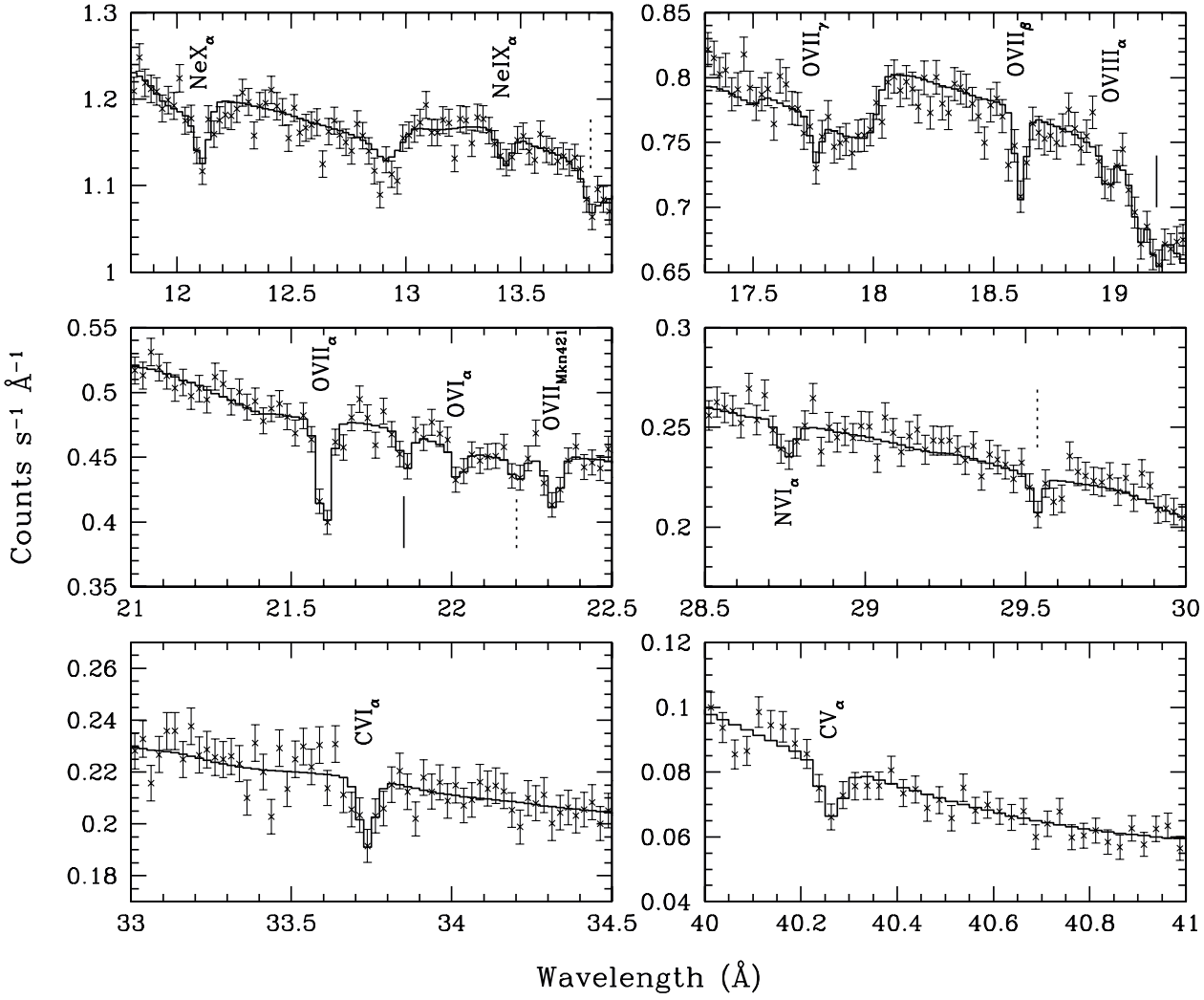

FIG. 1.—Portions of the Mrk 421 *Chandra* LETG spectrum (*crosses*) and the best-fitting model (*histogram*). Absorption lines at $z \sim 0$ are labeled, and vertical tick marks indicate absorption from the $z = 0.011$ (*solid*) and 0.027 (*dotted*) intervening WHIM filaments (Nicastro et al. 2005b).

the Murphy et al. (1996) Green Bank H I 21 cm data as a velocity reference. They find four main components of H I emission with an $N_{\rm H}$-weighted average velocity of -31.7 km s^{-1}. In the *FUSE* spectrum, the Si II λ1020.699 and Ar I λ1048.220 lines are expected to trace the same gas as the H I emission. Each UV line was fitted with two Gaussian components in Sherpa, giving average velocity offsets of -30.9 and -34.9 km s^{-1}, respectively. These agree well with the H I data, although the slight difference between the Ar I and Si II measurements suggests at least a $\sim$4 km s^{-1} intrinsic wavelength uncertainty.

3. LINE MEASUREMENTS

To find and identify narrow absorption lines in the *Chandra* spectrum of Mrk 421, we visually inspected small (2–5 Å) regions of the spectrum, beginning around the rest wavelength of O VII$_{K\alpha}$ (21.602 Å) since this tends to be the strongest $z = 0$ X-ray absorption line (e.g., Nicastro et al. 2002; Fang et al. 2003; Chen et al. 2003). Three O VII$_{K\alpha}$ (Fig. 1) absorption features were found: one at $z = 0$, one at $z = 0.011$, and one at $z = 0.027$ (with typical redshift errors of 0.001). There is also a strong feature that is $\sim$3 σ from the O V$_{K\alpha}$ rest wavelength but is more likely O VII$_{K\alpha}$ at $v \sim +900$ km s^{-1} relative to the blazar. A close pair of lines consistent with Lyα at this velocity has been observed (Shull et al. 1996; Penton et al. 2000), so this may be indicative of an inflow to Mrk 421 or uncertainty in the blazar redshift (based on rather old spectrophotometric measurements by Margon et al. 1978). A weak O VI$_{K\alpha}$ line is seen at the rest wavelength of 22.02 Å. Other regions of the spectrum were then searched for lines corresponding to these systems, with particular emphasis paid to strong transitions of the most abundant elements (C, N, O, and Ne). All in all there were 13 lines marginally or strongly detected at $z \sim 0$ (including the N VII, O V, and Ar XV upper limits), three at $z = 0.011$, and seven at $z = 0.027$. The latter two systems are the subject of other papers (Nicastro et al. 2005b, 2005c) and thus are not discussed further here.

These 13 $z = 0$ X-ray lines were fitted in Sherpa with narrow Gaussian features superposed on the fitted continuum described in § 2.1 (see Fig. 1). We are excluding the strong O I (λ23.51) line since it arises in the neutral interstellar medium (ISM) and is not of interest here, as well as the O_2 (λ23.34) absorption since it coincides with a strong instrumental feature and cannot be accurately measured. Due to the FWHM = 0.04 Å ($\sim$600 km s^{-1}) LETG resolution, the lines are all unresolved, so only the position and equivalent width of each line are measured. Errors are calculated using the "projection" command in Sherpa, allowing the overall continuum normalization to vary along with all parameters for each line. The resulting line parameter estimates are

TABLE 1
OBSERVED $z \sim 0$ LINES

Line ID	λ_{rest}[a] (Å)	λ_{obs}[b] (Å)	Δv_{FWHM} (km s^{-1})	v_{obs} (km s^{-1})	W_λ[c] (mÅ)	log N_i[c,d]	Notes
X-Ray							
Ar XV$_{K\alpha}$	24.737	24.737	...	...	<3.09	<15.12	
C V$_{K\alpha}$	40.268	40.26 ± 0.02	...	−60 ± 150	$11.3^{+3.3}_{-2.6}$	15.19 ± 0.15	
C VI$_{K\alpha}$	33.736	33.736 ± 0.02	...	0 ± 180	7.2 ± 1.4	15.31 ± 0.11	
Ne IX$_{K\alpha}$	13.447	13.431 ± 0.02	...	−360 ± 450	$2.4^{+0.9}_{-0.8}$	15.48 ± 0.24	
Ne X$_{K\alpha}$	12.134	$12.11^{+0.03}_{-0.02}$	...	-590^{+740}_{-490}	<5.04	<16.21	1
N VI$_{K\alpha}$	28.787	28.755 ± 0.02	...	−330 ± 210	4.1 ± 1.5	$15.02^{+0.19}_{-0.24}$	
N VII$_{K\alpha}$	24.781	24.781	...	...	<2.86	<15.16	
O V$_{K\alpha}$	22.374	22.374	...	...	<2.20	<14.97	2, 3
O VI$_{K\alpha}$	22.019	22.023 ± 0.02	...	50 ± 270	2.4 ± 0.9	$15.07^{+0.17}_{-0.22}$	2
O VII$_{K\alpha}$	21.602	21.603 ± 0.02	...	10 ± 280	9.4 ± 1.1	16.22 ± 0.23	
O VII$_{K\beta}$	18.629	18.612 ± 0.02	...	−273 ± 320	4.6 ± 0.7	16.28 ± 0.13	
O VII$_{K\gamma}$	17.768	17.762 ± 0.02	...	−100 ± 340	2.0 ± 0.7	$16.19^{+0.16}_{-0.21}$	
O VIII$_{K\alpha}$	18.969	18.974 ± 0.02	...	80 ± 320	1.8 ± 0.7	$15.17^{+0.16}_{-0.24}$	
UV							
O VI$_{1032}$	1031.926	1031.88 ± 0.01	152.3 ± 7.0	−13.7 ± 2.6	270.9 ± 7.9	14.43 ± 0.02	
O VI$_{1032,HVC}$	1031.926	1032.30 ± 0.04	59^{+31}_{-17}	108 ± 12	18.5 ± 5.6	$13.18^{+0.12}_{-0.16}$	
O VI$_{1037}$	1037.617	1037.59 ± 0.01	145.4 ± 11.6	−9.3 ± 4.0	164.9 ± 8.4	14.47 ± 0.03	

NOTES.—(1) The Ne X line lies within a detector feature, so only an upper limit on its equivalent width is given. (2) The O VI and O V λ_{rest} values are from laboratory measurements by Schmidt et al. (2004); theoretical oscillator strengths are taken from Pradhan et al. (2003). (3) There is an absorption line at −760 km s^{-1} from the O V rest wavelength, but this is more likely O VII associated with Mrk 421.

[a] From Verner et al. (1996), except O VI and O V, which are from Schmidt et al. (2004).

[b] Wavelength uncertainty is measured from fit or intrinsic LETG 0.02 Å error, whichever is greater. For upper limits, the line position was frozen to the rest wavelength.

[c] Error bars are 1 σ; upper limits are 2 σ.

[d] Column densities are calculated using curve-of-growth analysis with $b = 80.6 \pm 4.2$ km s^{-1} for C V, N VI, and O V, and the O VII Doppler parameter of $b = 31-46$ km s^{-1} (1 σ range) for all other lines.

presented in Table 1. The ∼0.02 Å systematic wavelength uncertainty of the LETG[13] is in most cases larger than the statistical uncertainty of the line centroid; thus, Table 1 lists whichever is greater. In addition, a meaningful upper error bar on the C VI equivalent width could not be calculated with Sherpa. In this case, the FWHM was frozen at the instrumental resolution and the error was recalculated; a visual inspection confirms the new limit to be more reasonable. Upper limits for the O V, N VII, Ar XV, and Ne X lines were calculated with both the position and FWHM frozen.

The *FUSE* spectrum (Fig. 2) shows a strong, broad, low-velocity O VI λ1032 absorption line at $z \sim 0$ due to gas in the Galactic thick disk and halo (Savage et al. 2003). An asymmetric wing on the red side of this line is evident, possibly a kinematically distinct HVC. We fitted the O VI λ1032 line in Sherpa using a constant local continuum (in a ±2 Å window) and two Gaussian absorption components: one for the $v \sim 0$ O VI$_{LV}$ line, and one at $v \sim 100$ km s^{-1} for the HVC. No H_2 contamination is seen at the O VI λ1032 wavelength when absorption templates are fitted to the other H_2 lines seen in the spectrum. The λ1037 line is somewhat blended with a single H_2 absorption line; this is taken into account with another narrow Gaussian. From this fit, we find equivalent widths of 18.6 ± 5.6 mÅ for the λ1032 HVC and 270.7 ± 7.9 mÅ for the Galactic component. The best-fit model for the HVC is fairly robust and not sensitive to variations in the initial parameters; however, the derived equivalent width of 18.5 ± 5.6 mÅ is lower than the 37 ± 11 ± 29 mÅ (errors are statistical and systematic, respectively) measured by Wakker

[13] See http://cxc.harvard.edu/cal.

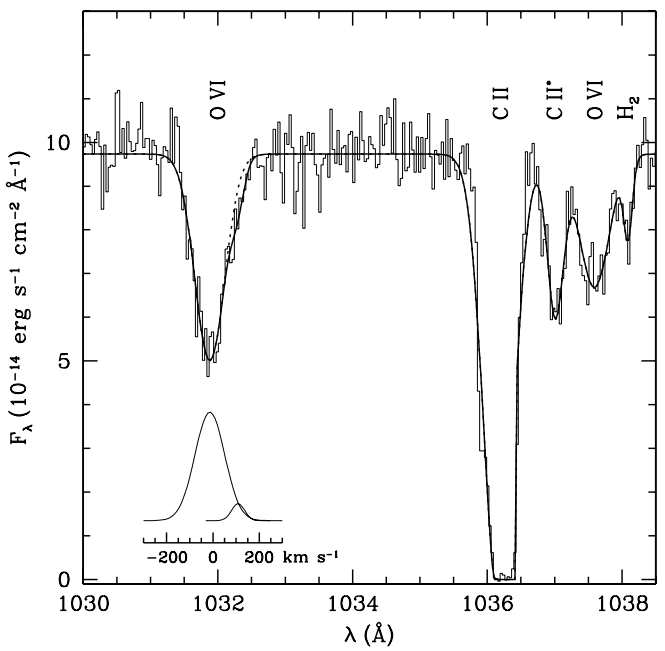

FIG. 2.—*FUSE* spectrum of Mrk 421 around the O VI $\lambda\lambda$1032, 1037 absorption doublet (*histogram*). The thick line shows the best-fit model with (*solid line*) and without (*dotted line*) the λ1032 HVC included. The inset plot shows the best-fitting Galactic (large Gaussian) and high-velocity (small Gaussian) components for the λ1032 line, plotted against velocity relative to the O VI rest wavelength.

et al. (2003) in the initial 21.8 ks observation. They employed a direct integration method that may not have taken into account the substantial blending of the Galactic O VI$_{LV}$ with the HVC. Our total O VI equivalent width (LV + HVC = 279 ± 10 mÅ) is in good agreement with their value of 285 ± 20 mÅ.

Deblending the O VI λ1037 line is less certain due to the presence of adjacent Galactic C II and H_2 absorption. A flat continuum was again employed from 1035 to 1040 Å and single Gaussian components were used to fit the C II, O VI, and H_2 absorption lines. The HVC on the O VI λ1032 line should also appear at ~1038 Å with $W_\lambda = 0.50 W_\lambda$(1032 Å). Although this component is too weak to be detected directly, it could cause the measurement of the Galactic LV O VI λ1037 line to be systematically high. Another absorption Gaussian with one-half of the λ1032 HVC equivalent width (and with the same FWHM and velocity offset) was included in the O VI λ1037 line fit to account for this. Table 1 lists the measured properties of the O VI$_{LV}$ and HVC absorption lines.

4. ABSORPTION-LINE DIAGNOSTICS

4.1. *Doppler Parameters*

To convert the measured equivalent widths to ionic column densities, we calculated curves of growth for each absorption line over a grid of Doppler parameters (b = 10–100 km s^{-1}) and column densities [log N_H(cm^{-2}) = 12.0–18.0], assuming a Voigt line profile. Since the X-ray lines are unresolved, b cannot be measured directly. It can, however, be inferred from the relative strengths of the three measured O VII K series lines. These lines are produced by the same ionic species, so in an unsaturated medium $W_\lambda \propto f_{lu}\lambda^2$, where f_{lu} is the oscillator strength. The expected equivalent width ratio of O VII Kβ to Kα is then W_λ(Kβ)/W_λ(Kα) = 0.156, so the measured value of 0.49 ± 0.09 indicates that the Kα line is saturated. On the other hand, the measured O VII Kγ/Kβ ratio is 0.43 ± 0.16, in agreement with the predicted (unsaturated) value of 0.34.

These line ratios by themselves are insufficient to determine the physical state of the O VII–absorbing medium since b and $N_{O\,VII}$ are degenerate: the Kα line saturation could be due to high column density, low b, or a combination of both. However, given an absorption line with a measured equivalent width and known $f_{lu}\lambda^2$ value, the inferred column density as a function of the Doppler parameter can be calculated. The measured equivalent width (and errors) for each transition thus defines a region in the $N_{O\,VII}$-b plane. Since the actual value of $N_{O\,VII}$ is fixed, b and $N_{O\,VII}$ can be determined by the region over which the contours "overlap," i.e., the range of Doppler parameters for which the different transitions provide consistent $N_{O\,VII}$ measurements.

Figure 3 shows such 1 σ contours for the three measured O VII transitions. As expected, the inferred $N_{O\,VII}$ is nearly constant in the unsaturated regime (large b) and rises sharply at low b as the lines begin to saturate. At each value of b, the differences $\Delta(\log N_{\alpha\beta}) = \log N_{K\alpha} - \log N_{K\beta}$ and $\Delta(\log N_{\alpha\gamma}) = \log N_{K\alpha} - \log N_{K\gamma}$ were calculated, along with the errors on each $\Delta(\log N)$. The quantity $\Delta(\log N_{\alpha\beta})$ is consistent with zero at the 1 and 2 σ levels for 15 km s^{-1} < b < 46 km s^{-1} and 13 km s^{-1} < b < 55 km s^{-1}, respectively, while $\Delta(\log N_{\alpha\gamma})$ provides limits of 31 km s^{-1} < b < 50 km s^{-1} and 24 km s^{-1} < b < 76 km s^{-1}, respectively. Since $\Delta(\log N_{\alpha\gamma})$ provides a more stringent lower limit on b while $\Delta(\log N_{\alpha\beta})$ better constrains the upper limit, we thus assume a 1 σ range of 31 km s^{-1} < b < 46 km s^{-1} and a 2 σ range of 24 km s^{-1} < b < 55 km s^{-1}. It should be noted that Figure 3 also shows some overlap between the Kα and Kγ

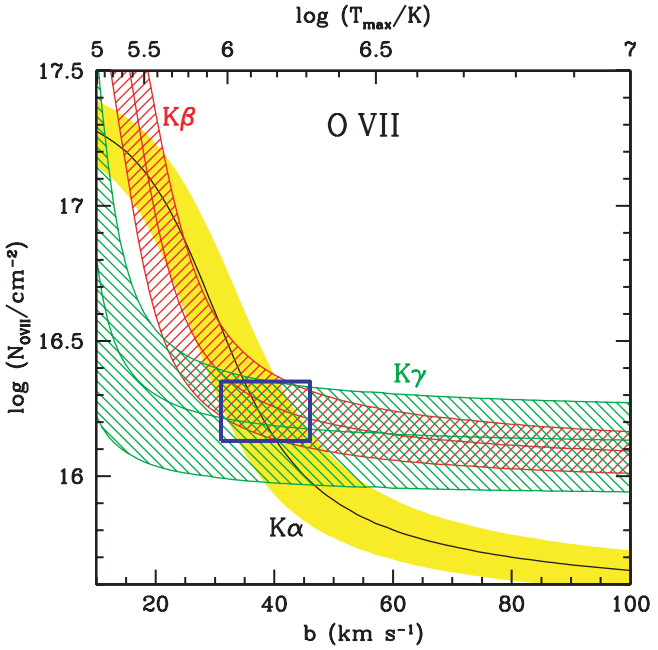

FIG. 3.—Contours of allowed $N_{O\,VII}$ and b for the O VII Kα (*yellow*), Kβ (*red*), and Kγ lines. Shaded regions depict the 1 σ errors on W_λ, with the best-fit W_λ line in the center of each region. The overlap between the Kα and Kγ regions provides a 2 σ lower limit of b > 24 km s^{-1}, and the Kα-Kβ overlap implies b < 55 km s^{-1}. The weighted average O VII column density of the three transitions over the 1 σ b range is log ($N_{O\,VII}$) = 16.24 ± 0.11. The blue box depicts the 1 σ ranges in log ($N_{O\,VII}$) and b. Also labeled on the top axis is log T_{max} = log ($mb^2/2k$), the temperature inferred from a given Doppler parameter assuming purely thermal motion.

at $b \lesssim 12$ km s^{-1}; however, this solution is unlikely given the lower limit provided by the Kβ line. Moreover, b = 12 km s^{-1} implies a maximum temperature (assuming purely thermal motion) of $T_{max} = 1.3 \times 10^5$ K; such a low temperature is unlikely to produce the observed strong high-ionization lines.

A similar analysis is not as effective when applied to the strong O VI$_{LV}$ UV doublet (from the thick disk), since these lines are only slightly saturated: the measured W_λ ratio is 0.61 ± 0.04, compared to the expected unsaturated value of 0.50. When the inferred $N_{O\,VI}$ is calculated as a function of b for both lines of the O VI$_{LV}$ doublet, the predicted $N_{O\,VI}$ values are consistent over b = 34–112 km s^{-1} (at the 2 σ level; see Fig. 4). Since the O VI$_{LV}$ λ1032 line is fully resolved by *FUSE* (~15 resolution elements across the line profile) and relatively unblended, its Doppler parameter can be estimated much more accurately using the measured line width and strength. In an unsaturated absorption line, FWHM = 2(ln 2)$^{1/2}b$; however, the measured FWHM increases if the line is saturated. We compensated for this by calculating Voigt profile FWHMs on a grid of $N_{O\,VI}$ and b and determining the region consistent with the O VI$_{LV}$ λ1032 FWHM measurement of 152 ± 7 km s^{-1} (or b = 91 ± 4 km s^{-1} assuming no saturation).

When the FWHM-derived contour is overlaid on the $N_{O\,VI}$-b contour inferred from the equivalent width measurement of the LV O VI λ1032 line, the two regions overlap nearly orthogonally (Fig. 4), leading to a constraint of b(O VI$_{LV}$) = 80.6 ± 4.2 km s^{-1}. This is ~2 σ lower than the unsaturated FWHM, once again confirming that the O VI$_{LV}$ is only weakly saturated. At this b the inferred column densities from the two lines of the O VI$_{LV}$ doublet differ by 1.3 σ, but this is only a minor discrepancy and likely due to errors introduced by the blending of the λ1037 line; thus, we only consider results from the more reliable

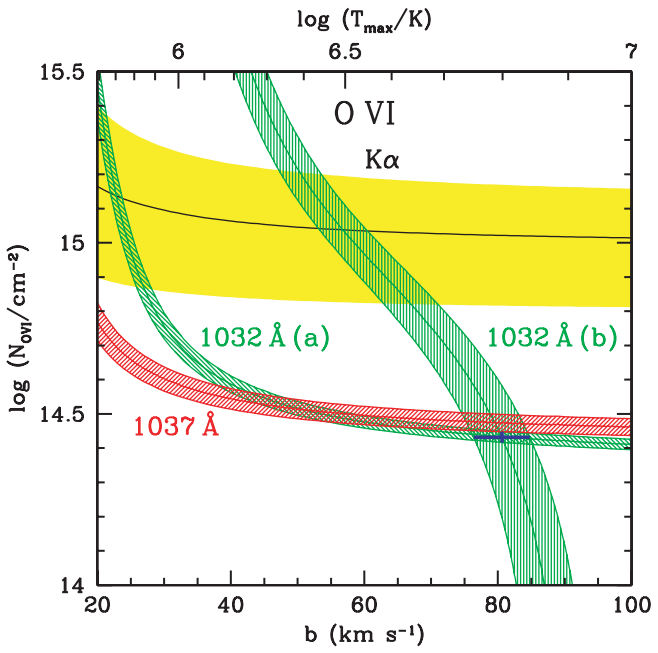

FIG. 4.—Contours of allowed $N_{\rm O\ VI}$ and b for the O VI λ1032 (*green*), λ1037 (*red*), and putative Kα λ22 (*yellow*) lines. Contour *a* is derived from the O VI$_{\rm LV}$ λ1032 equivalent width, while contour *b* is from the measured FWHM; the intersection between the two green contours provides a tight constraint of $b = 80.6 \pm 4.2$ km s^{-1} and $\log N_{\rm O\ VI}({\rm cm}^{-2}) = 14.432 \pm 0.016$ for the O VI$_{\rm LV}$ (*blue cross*). Note that the O VI Kα transition predicts $N_{\rm O\ VI}$ about 0.5 dex higher than the UV line, and this discrepancy cannot be explained by saturation.

λ1032 line measurement. However, at no value of the Doppler parameter do the λ1032, λ1037, and O VI$_{\rm K\alpha}$ lines all produce a consistent $N_{\rm O\ VI}$ measurement; in fact, the O VI$_{\rm K\alpha}$ column density is a factor of $\sim$4 higher than that inferred from the UV data. This discrepancy is discussed further in § 5.1.1.

4.2. *Column Densities*

The Doppler parameters measured for the O VII (31 km s^{-1} $< b <$ 46 km s^{-1}) and O VI$_{\rm LV}$ ($b = 80.6 \pm 4.2$ km s^{-1}) absorption are inconsistent at the $\sim$3 σ level, indicating the presence of at least two distinct components: the Galactic thick-disk gas traced by broad $v \sim 0$ O VI$_{\rm LV}$ absorption, and another lower b phase, possibly of extragalactic origin, traced by the O VII absorption lines. It cannot be assumed a priori that any given line (other than those used to determine b) originates in one phase or another; moreover, the uncertainty in the calculated column density depends on not only the equivalent width error but also the error in b. To take this into account, for each ion the derived column density $\log N_i$ and its ± 1 σ limits were averaged over the ± 1 σ ranges of both measured Doppler parameters. As it turns out, the choice of b does not make a significant difference since all other lines (besides the O VII and O VI$_{\rm LV}$ absorption) are essentially unsaturated; i.e., the difference in N_i calculated with the O VI$_{\rm LV}$ and O VII Doppler parameters is small compared to the 1 σ error on the equivalent width measurements. Even so, to avoid possible systematic errors, we assumed $b = 80.6 \pm 4.2$ km s^{-1} for those lines *likely* to originate in the Galactic thick disk (O VI$_{\rm LV}$, O V, and C V) and $b = 31$–46 km s^{-1} for all other species. The derived ionic column densities are listed in Table 1.

4.3. *Temperature and Density Constraints*

At densities such as those found in the Galactic ISM ($n_e \sim 1$ cm^{-3}), photoionization is unimportant because thermal collisions are by far the dominant ionization source. This is also the case for very high temperatures ($T \gtrsim 10^7$ K) even at low densities, since the collisional rate is greater than the photoionization rate. However, at the low densities typically found in the IGM ($n_e = 10^{-6}$ to 10^{-4} cm^{-3}), photoionization from the diffuse UV/X-ray background begins to play a greater role by enriching the abundances of highly ionized elements at typical WHIM temperatures [$\log T({\rm K}) \sim 5$–7] relative to those expected from pure collisional ionization (Nicastro et al. 2002; Mathur et al. 2003). It is thus imperative that the ionizing background be taken into account in order to accurately predict ionic abundances in the WHIM.

Version 90.04 of the ionization balance code CLOUDY (Ferland 1996) was used to compute collisional plus photoionization hybrid models for the absorbing medium. Relative ionic abundances were computed over a grid of $\log T({\rm K}) = 4.5$–7.4 and $\log n_e({\rm cm}^{-3}) = -7$ to 0, with a step size of 0.1 dex in both $\log n_e$ and $\log T$. Initially, a rigid scaling of $[{\rm Z/H}] = -1$ for all metals was assumed. For the ionizing background we employed the Sternberg et al. (2002) fit to the metagalactic radiation field:

$$J_\nu = \begin{cases} J_{\nu 0}\left(\dfrac{\nu}{\nu_0}\right)^{-3.13}, & 1 < \dfrac{\nu}{\nu_0} < 4, \\ 2.512\times 10^{-2} J_{\nu 0}\left(\dfrac{\nu}{\nu_0}\right)^{-0.46}, & \dfrac{\nu}{\nu_0} > 4, \end{cases} \quad (1)$$

where here $J_{\nu 0} = 2\times 10^{-23}$ ergs s^{-1} cm^{-2} Hz^{-1} sr^{-1} and $\nu_0 =$ 13.6 eV. The total flux of ionizing photons is then given by $f_\gamma = 4\pi \int_{\nu_0}^{\infty} (J_\nu/h\nu)\, d\nu = 1.3\times 10^4$ photons s^{-1} cm^{-2}, and the ionization parameter is $\log U = \log (f_\gamma/c) - \log n_e = -6.36 - \log n_e$, where n_e is the electron density in cm^{-3}.

Using the ionic abundances calculated with CLOUDY, we derived expected abundance ratios for all observed ions at each point in the $\log n_e$–$\log T$ plane. Since any given density and temperature uniquely determine a set of abundance ratios (N_a/N_b for all ions a and b), the problem can be inverted: any value of N_a/N_b defines a curve in the $\log n_e$–$\log T$ plane, i.e., a set of temperatures and densities that can produce the measured ratio. When the errors on N_a/N_b are taken into account, the curves become contours, and the overlap between two or more contours defines the temperatures and densities for which the measured ratios are consistent. This is analogous to the method used in § 4.1 to determine Doppler parameters for O VI$_{\rm LV}$ and O VII.

The most powerful diagnostics are those using ratios between different ions of the same element, since these ratios are independent of the relative metal abundances. Unfortunately, the N VII/N VI and Ne X/Ne IX upper limits are not stringent enough to place meaningful constraints on the temperature and density. Figure 5 shows the $\log n_e$–$\log T$ contours for ratios between the X-ray O VI$_{\rm K\alpha}$, O VII, and O VIII lines, as well as the O VI$_{\rm HVC}$/O VII ratio. The X-ray line ratios are inconsistent with a high-density ($n_e \gtrsim 10^{-3}$cm^{-3}), high-temperature ($\log T > 6.2$) medium and instead converge on a partially photoionized plasma with $n_e = 10^{-4.7}$ to $10^{-3.9}$ cm^{-3} (from the overlap between the O VI$_{\rm K\alpha}$/O VII and O VIII/O VII contours) and $T = 10^{5.5}$–$10^{5.7}$ K (from the limits provided by O VI$_{\rm K\alpha}$/O VII in this density range). These ranges of temperatures and densities are in line with those expected from WHIM gas (Davé et al. 2001). Of course, this is all contingent on the O VI$_{\rm K\alpha}$ line being a reliable tracer of $N_{\rm O\ VI}$; this caveat is discussed in detail in § 5.

On the other hand, the O VI$_{\rm HVC}$/O VII ratio overpredicts the temperature by at least an order of magnitude for all values of $\log n_e$: in order to be consistent with the O VIII/O VII ratio, the

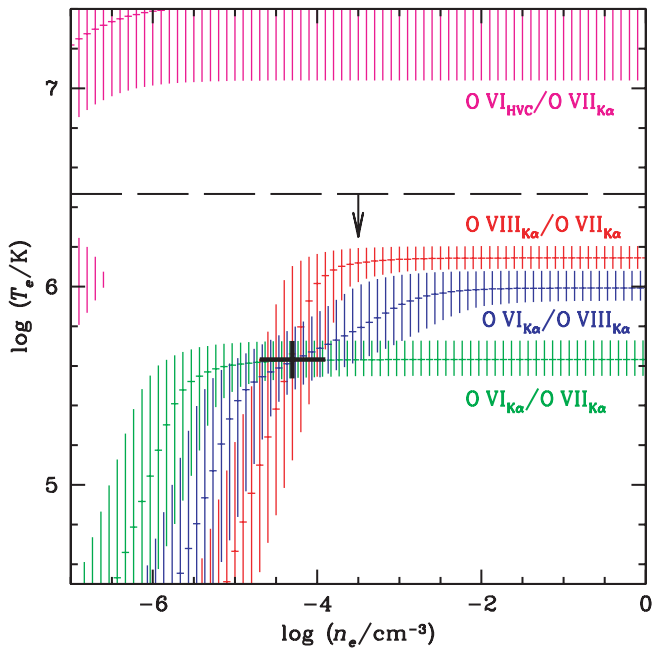

FIG. 5.—Contours of constant abundance ratios for X-ray and UV oxygen absorption lines. Vertical bars denote the 2 σ range of temperatures inferred from the abundance ratio at each step in log n_e. The horizontal dashed line is the 2 σ upper limit on the temperature of the O VII absorber from the Doppler parameter measurement. While the X-ray line ratios predict significantly different temperatures in the collisional ionization regime ($\log n_e \gtrsim -3$), they are consistent with $\log n_e(\mathrm{cm}^{-3}) = -4.7$ to -3.9 and $\log T(\mathrm{K}) \sim 5.5$–$5.7$ (*black cross*). Note that the O VI$_{HVC}$/O VII ratio predicts a temperature far higher than the other derived limits, and thus the HVC is unlikely to be associated with the O VII absorption.

O VI$_{HVC}$/O VII ratio would need to be stronger by a factor of $\sim$2.5 (or $\sim$3.5 σ). It is possible that the HVC is not a physically distinct component but is instead the result of some systematic error (such as fixed pattern noise or an unexpected anomaly in the Galactic O VI$_{LV}$ velocity distribution). In this case, the O VI associated with the O VII and O VIII may be completely blended with the thick-disk O VI$_{LV}$ and thus unmeasurable. Consistency with the O VIII/O VII ratio (in the collisional ionization regime) requires $\log (N_{\mathrm{O\ VI}}/N_{\mathrm{O\ VII}}) \sim -2.5$, or roughly 20% of the Galactic UV O VI absorption. Although it appears that the O VI HVC as measured cannot originate in the same medium as the O VII absorption, we suspect that additional atomic physics may be at work here and could in principle reconcile this disagreement (see § 5.1.1).

While the O VI$_{K\alpha}$/O VII and O VIII/O VII ratios provide strong constraints, it is important to consider other ion ratios as well (particularly since the O VI$_{K\alpha}$ and O VI λ1032 column densities disagree). Figure 6 shows the log n_e– log T contours for several different ion ratios, all calculated relative to O VII since the error on $N_{\mathrm{O\ VII}}$ is small. With a rigid metallicity shift relative to solar, the Ne IX/O VII, O VIII/O VII, and O VI$_{K\alpha}$/O VII ratios are not all consistent with each other for any combination of temperature and density; however, the consistency can be improved with adjustments to the [Ne/O] ratio (see § 5.1.3). Both the C VI/O VII and N VII/O VII measurements are consistent with a high- or low-density medium at solar abundances.

Limits on the temperature of the Galactic thick-disk absorption can be derived in a similar fashion, although it is not the primary focus of this work and there are far fewer measured lines to work with. The most accurately measured line is the O VI$_{LV}$; in addition, C V and N VI X-ray lines are measured, and upper limits have been determined for O V and N VII. Figure 7 shows the temperature constraints derived for this Galactic absorption, assuming pure collisional ionization. The O V/O VI$_{LV}$ and N VII/N VI upper limits provide metallicity-independent constraints of

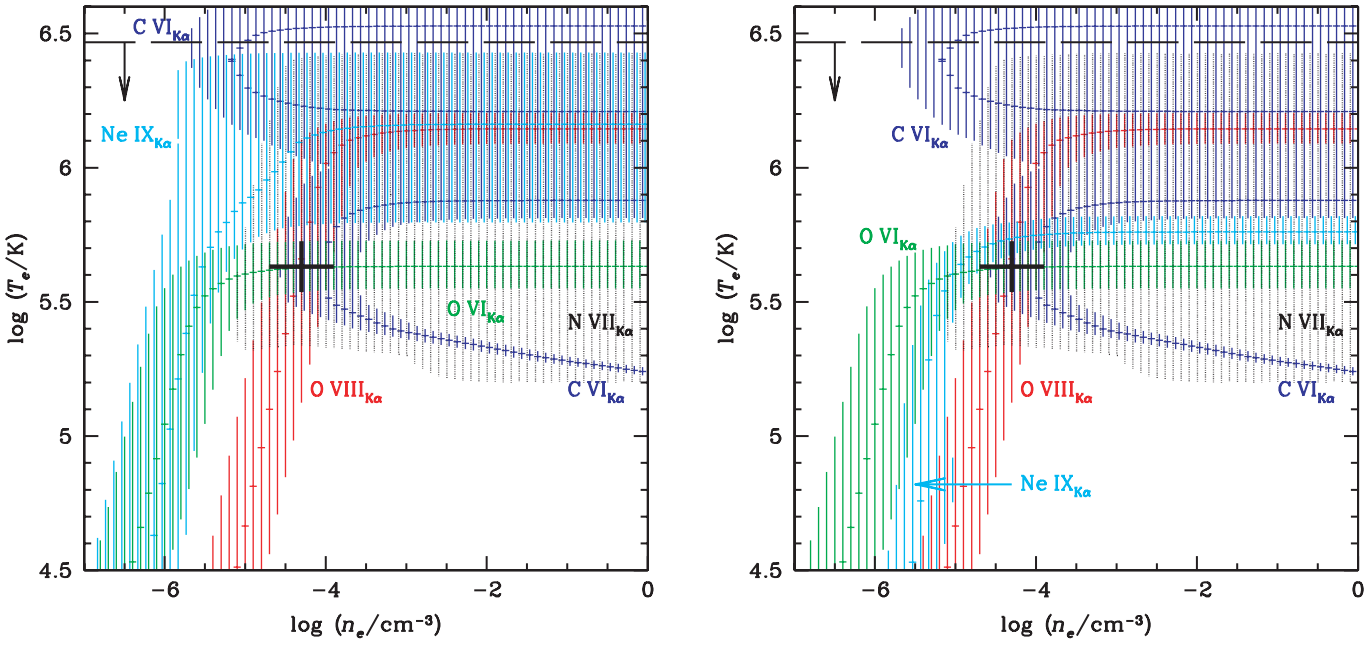

FIG. 6.—Same as Fig. 5, but for ratios of several different ion abundances to O VII: O VI$_{K\alpha}$ (*green*), O VIII (*red*), C VI (*blue*), Ne IX (*cyan*), and N VII (*dotted black region*). The black cross shows the range of log T and log n_e derived from the O VIII/O VII and O VI$_{K\alpha}$/O VII ratios. Assuming solar abundances (*left panel*), the O VI$_{K\alpha}$ and Ne IX contours are inconsistent for $\log n_e \gtrsim -5$, while all other ratios (except O VI$_{K\alpha}$/O VII) are consistent at $\log n_e \gtrsim -4.5$. The right panel shows how a neon abundance shift of [Ne/O] = 1 produces better agreement in the low-density regime. High-density models agree with the data only if the O VI$_{K\alpha}$ measurement is disregarded.

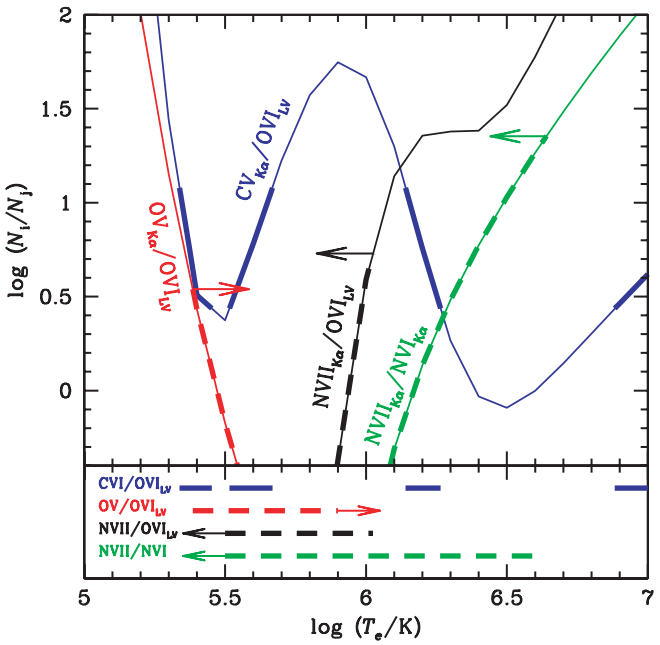

FIG. 7.—Models of ionic column density ratios for ions likely to arise in the Galactic ISM (assuming pure collisional ionization). Calculated ratios are shown by thin lines with $\pm 2\ \sigma$ ratio measurements overplotted (*thick segments*). Upper limits are shown by dashed lines, and the temperature ranges derived from the different ion ratios are shown in the bottom panel. The same-element ratios in this case provide strong constraints of $\log T > 5.4$ (O V/O VI) and $\log T < 6.6$ (N VII/N VI).

$\log T > 5.39$ and $\log T < 6.64$, respectively. A more stringent upper limit on temperature of $\log T < 6.03$ is provided by the N VII/O $\mathrm{VI_{LV}}$ ratio, but this is somewhat dependent on [N/O]. Within this range the C V/O $\mathrm{VI_{LV}}$ ratio provides an even stricter limit of $5.3 < \log T < 5.7$, but again this depends on [C/O]. At these temperatures the expected O VII column density is at most an order of magnitude less than measured; thus, the O $\mathrm{VI_{LV}}$, O VII, and O VIII cannot all originate in the same phase assuming pure collisional ionization (see also Mathur et al. 2003).

5. DISCUSSION

Our *Chandra* and *FUSE* observations have provided a wealth of data on absorption near the Galaxy, constraining the temperature and density tightly [$\log T(\mathrm{K}) = 5.5$–5.7 and $n_e = 10^{-4.7}$ to $10^{-3.9}$ cm^{-3} when the O $\mathrm{VI_{K\alpha}}$ measurement is included], which are conditions suggestive of the Local Group IGM and require supersolar [Ne/O]. Here we first examine the assumptions that have led us to these results (§ 5.1), and then we discuss their implications for the location of the absorbing gas (§ 5.2), subject to these caveats.

5.1. *Potential Caveats*

5.1.1. *The* O VI *Discrepancy*

The interpretation of the UV and X-ray data is particularly important, since (as Fig. 5 shows) the combined O VIII/O VII and O VI/O VII ratios can provide tight constraints on the absorber temperature and density simultaneously (see also Fig. 5 in Mathur et al. 2003). However, in this case the O VI column density inferred from the O $\mathrm{VI_{K\alpha}}$ is a factor of $\sim$4 higher than the combined λ1032 low- and high-velocity components. Since both the X-ray and UV transitions trace the same atomic state, the inferred column densities should match. A similar disagreement has been seen in intrinsic active galactic nucleus (AGN) absorption systems (see Krongold et al. 2003; Arav et al. 2003); however, in these cases it is typically attributed to saturation or a velocity-dependent covering factor, neither of which is relevant to this $z \sim 0$ absorption.

On the other hand, our O $\mathrm{VI_{K\alpha}}$ measurement provides a test for these attributions; the local absorption, after all, is likely a dramatically different physical system than an AGN outflow, yet the same conflict arises. A macroscopic explanation does not adequately describe how this discrepancy is seen in both physical systems, so the actual reason may lie in the atomic physics of highly ionized plasmas. For example, some fraction of the O VI may be excited through collisions or recombination from O VII and thus unable to produce λ1032 absorption while still absorbing O $\mathrm{VI_{K\alpha}}$ photons. While a scenario that produces significant depopulation of the O VI ground state is difficult to envisage in such a low-density plasma, we are investigating further the statistical equilibrium of O VI including photoexcitation and recombination in order to study such effects in more detail. However, it should be emphasized that this is not an isolated case so there must be a physical explanation for the O VI discrepancy, and the resolution of this paradox is crucial to our understanding of O VI UV and X-ray absorption and how it relates to the O VII.

There is also the possibility that the line was misidentified as O $\mathrm{VI_{K\alpha}}$ and is actually another intervening O VII absorption line at $z = 0.0195$. The latter explanation is unlikely since no other absorption lines at this redshift are seen in the *FUSE* or *Chandra* spectra; in addition, this would require the line to fall exactly on the O VI rest wavelength, which seems like an improbable coincidence. Another possibility is that the theoretical oscillator strength of the O $\mathrm{VI_{K\alpha}}$ transition is incorrect, but the value given in Pradhan (2000) would need to be low by a factor of $\sim$2–4, in sharp contrast to the successful calculations of f_{lu} for inner-shell transitions in other ions in the same paper. Nevertheless, due to the discrepancy between the UV and X-ray O VI column density measurements, we present both possibilities: either (*a*) the O $\mathrm{VI_{K\alpha}}$ line measures $N_{\mathrm{O\ VI}}$, or (*b*) it does not and is thus ignored.

5.1.2. *Absorption Components*

The Doppler parameter measurements indicate the existence of two distinct components along the Mrk 421 line of sight: one seen in the thick-disk O $\mathrm{VI_{LV}}$ λ1032 absorption with $b_{\mathrm{LV}} = 80.6 \pm 4.2$ km s^{-1}, and the O VII absorber with $b_{\mathrm{O\ VII}} = 31$–46 km s^{-1} ($1\ \sigma$ limits). The O VI HVC may represent a third phase (if case *b* above is correct) with $b_{\mathrm{HVC}} = 35^{+18}_{-10}$ km s^{-1} (from the FWHM measurement). This agrees surprisingly well with the O VII *b* measurement and is consistent with numerical simulations of the nearby IGM (Kravtsov et al. 2002). However, the extremely low O $\mathrm{VI_{HVC}}$/O VII ratio requires a temperature much higher than the upper limit provided by $b_{\mathrm{O\ VII}}$. In order for the HVC to trace the same gas as O VII (case *a*), the aforementioned atomic physics effects would need to be suppressing O VI HVC absorption and not the O $\mathrm{VI_{LV}}$ line. Sembach et al. (2003) list mean Doppler parameters for a variety of HVCs, both Galactic and probable Local Group; unfortunately, the dispersion in these values and the errors on $b_{\mathrm{O\ VII}}$ and b_{HVC} measured here are both too large to associate the components presented here with one of their classifications.

It is also important to note that our analysis assumes a single-phase origin for the included X-ray lines. This assumption is consistent with the data, given the good agreement between the three O VII lines in the calculated ranges of *b* and $N_{\mathrm{O\ VI}}$ (Fig. 3). Even so, if any of the ionic species arise in more than one phase

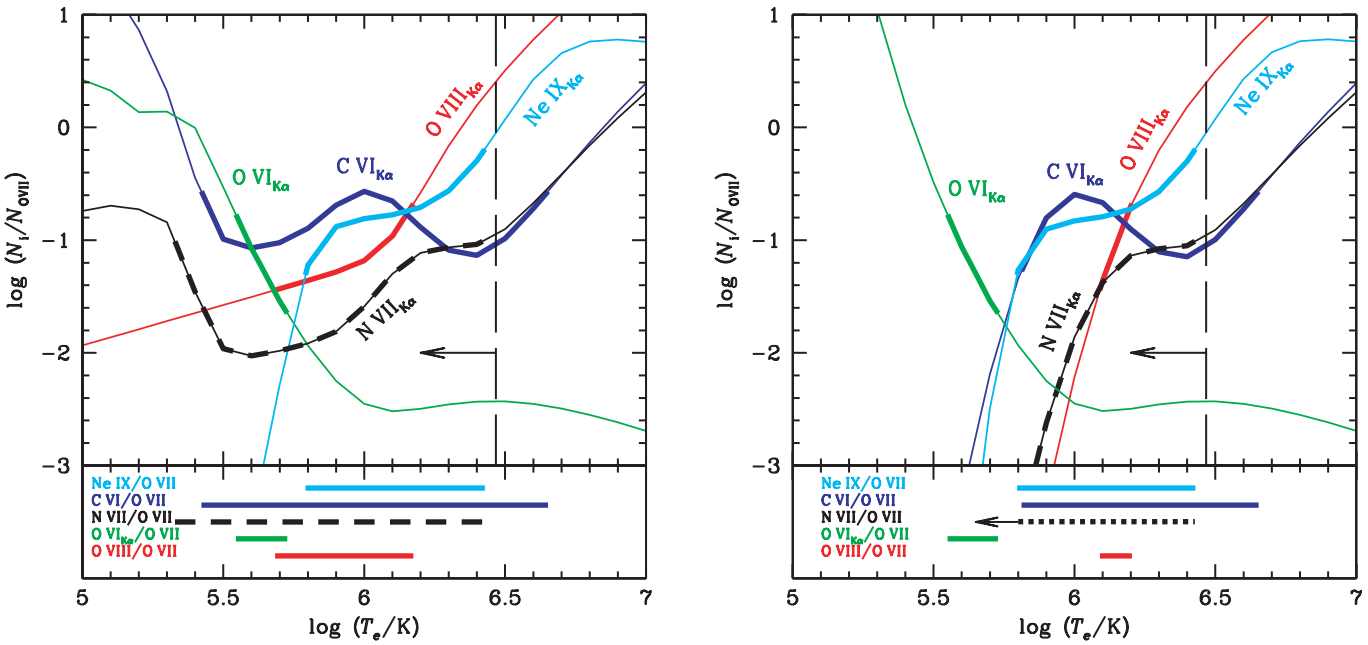

FIG. 8.—Same as Fig. 7, but for the ions likely originating in an extragalactic medium, with $\log n_e = -3.9$ (*left*) and $\log n_e = 0$ (*right*). Solar abundances relative to oxygen are assumed, and all calculated ratios are relative to $N_{\rm O\ VII}$. The low-density case produces a consistent temperature solution of $T \sim 10^{5.7}$ K (from the overlap between the O VIII and O VI$_{K\alpha}$ bold regions), and [Ne/O] must be supersolar. The high-density case, on the other hand, provides a consistent solution with solar abundances, but the temperatures implied by the O VIII/O VII and O VI$_{K\alpha}$/O VII ratios are inconsistent.

along the line of sight, our results could be affected. For example, a Galactic, purely collisionally ionized medium can in principle reproduce the observed relative abundances of O VIII, O VII, O VI$_{K\alpha}$, and Ne IX if several unresolved components are invoked to explain this absorption. However, the simplest explanation (a single-phase, low-density, partially photoionized extragalactic absorber) is fully consistent with all of these line measurements, and the similarity of the derived absorber properties to expectations for the local WHIM lends further support to this model (see § 5.2).

5.1.3. *Abundances*

Due to the uncertainty associated with the O VI$_{K\alpha}$ absorption, metal abundances relative to oxygen play a particularly important role in this analysis. By adjusting the metal abundances of the absorbing gas, the consistency of the solutions can in principle be improved with and without the O VI$_{K\alpha}$ measurement. Although the $\log n_e$– $\log T$ contour plots are useful for finding solutions, they cannot easily be used to determine the effects of changes in elemental abundances; thus, Figure 8 shows $N_i/N_{\rm O\ VII}$ as a function of $\log T$ for both the $\log n_e = -3.9$ and $\log n_e = 0$ cases. In this figure, the *y*-ranges given by the measured ratios (*thick lines*) shift up and down as a result of decreases and increases in the abundances relative to oxygen, respectively; thus, different parts of the theoretical curves would be in bold, moving the allowed temperature ranges (shown in the bottom panel) to the left or right. Solar abundances here are taken to be the CLOUDY 90 defaults (Ferland 1996; Grevesse & Anders 1989).

In case *a*, i.e., if the O VI$_{K\alpha}$ measurement of $N_{\rm O\ VI}$ is correct, then the temperature and density of the absorber are tightly constrained in a metallicity-independent manner, and relative abundances for other elements can be estimated. Under this assumption, the oxygen ion ratios are consistent within a range of $n_e = 10^{-4.7}$ to $10^{-3.9}$ cm^{-3}; however, at solar abundances the Ne IX/O VII ratio demands higher temperatures than allowed by the O VI$_{K\alpha}$/O VII ratio. Over this range of densities, the permitted abundances of neon, carbon, and nitrogen abundances relative to oxygen (that is, the range of abundances that produce line ratios consistent with both O VI$_{K\alpha}$/O VII and O VIII/O VII) are then $0.6 \leq [{\rm Ne/O}] \leq 2.2$, $-0.8 \leq [{\rm C/O}] \leq 0.3$, and $[{\rm N/O}] \leq 0.9$. Note that supersolar [Ne/O] has also been observed in the $z = 0$ absorber toward PKS 2155−304 (Nicastro et al. 2002). The improvement in the fit from supersolar [Ne/O] is shown in the right panel of Figure 6. Note, however, that in this case the discrepancy between the O VI$_{K\alpha}$ and λ1032 measurements becomes even more severe. Since the bulk of the O VI$_{\rm LV}$ cannot be associated with the O VII due to the different Doppler parameters, the UV O VI component associated with the WHIM (hence the O VI$_{K\alpha}$) must be substantially weaker than the Galactic O VI absorption; thus, the discrepancy is correspondingly larger.

On the other hand (case *b*), if the O VI$_{K\alpha}$ line is ignored, then the relative abundances in the absorber can be adjusted such that the measured line ratios are consistent with either a low- or high-density absorber. As shown in Figure 6, a high-density, collisionally ionized medium fits the data with solar abundances. Assuming that this is the case, the temperature is then completely constrained by the O VIII/O VII ratio at $\log T = 10^{6.1}$–$10^{6.2}$ K, and the relative abundances consistent with the O VIII/O VII ratio in this temperature range are $-0.6 \leq [{\rm Ne/O}] \leq 0.6$, $-0.6 \leq [{\rm C/O}] \leq 0.3$, and $[{\rm N/O}] \leq 0.4$.

The requirement that [Ne/O] be supersolar does not affect the viability of the partially photoionized model: in both the ISM and low-*z* IGM, [Ne/O] is observed to be significantly larger than the solar value (e.g., Paerels et al. 2001; Nicastro et al. 2005b). This may be an intrinsic property of the enriched gas ejected into the IGM and ISM or instead could be due to depletion of C, N, and O onto dust grains in supernova ejecta or quasar winds (Whittet 1992; Elvis et al. 2002). If the dust destruction timescale is long and the IGM is continuously enriched by this latter mechanism, then the observed supersolar [Ne/O] would be expected. All of these enrichment scenarios

are quite uncertain, but few (if any) are able to produce $[\mathrm{Ne/O}] < 0$. Indeed, the solar neon abundance itself is quite uncertain since it is inferred from solar wind measurements. The increase in the solar neon abundance proposed by Drake & Testa (2005) is supported by these observations and may provide another physical argument for the lack of subsolar [Ne/O].

5.2. *Where Does the X-Ray Absorption Originate?*

Assuming that the O VII absorption system is homogeneous, its radial extent can be estimated by calculating $r \approx N_{\mathrm{H}}/(\mu n_e)$, where $\mu \sim 0.8$, $\log(n_{\mathrm{O}}/n_{\mathrm{H}}) = -3.13$ (solar abundance), and

$$N_{\mathrm{H}} = N_{\mathrm{O\ VII}}\left(\frac{N_{\mathrm{O,tot}}}{N_{\mathrm{O\ VII}}}\right) \times 10^{3.13-[\mathrm{O/H}]}. \quad (2)$$

The second term in the equation is approximately unity, since over the range of temperatures and densities implied from the O VIII/O VII ratio, O VII is the dominant ionization state by at least an order of magnitude; thus, $\log N_{\mathrm{H}} = \log N_{\mathrm{O\ VII}} + 3.13 - [\mathrm{O/H}] = [20.37 - ([\mathrm{O/H}] + 1)] \pm 0.11$. The measurement error on $N_{\mathrm{O\ VII}}$ is small compared to the uncertainty range in n_e, so it can be disregarded. Assuming that the O VI$_{\mathrm{K}\alpha}$ line does measure $N_{\mathrm{O\ VI}}$, the 2 σ range of densities is $-4.7 \leq \log n_e \leq -3.9$, resulting in a radial extent of $r = (0.8\text{–}4.9) \times 10^{-([\mathrm{O/H}]+1)}$ Mpc. These radial extents are consistent with those expected from a Local Group medium or Local filament interpretation for this absorption (Nicastro et al. 2002, 2003) and too large to be confined within a Galactic halo. The absorber extent could be marginally consistent with a Galactic corona if the metallicity is high ($r = 80\text{–}490$ kpc, 2 σ limits at solar metallicity); however, such a scenario seems implausible, particularly if this corona primarily consists of gas accreted from the metal-poor IGM.

It is unlikely that this absorption system, if extragalactic, is spherically symmetric (particularly in a Local filament interpretation). The total mass in the O VII system can be written as $M_{\mathrm{tot}} = f(4/3)\pi r^3(1.4 n_{\mathrm{H}} m_{\mathrm{H}})$, where $f(<1)$ parameterizes the departure from spherical symmetry and $1.4 n_{\mathrm{H}} m_{\mathrm{H}} \approx n_{\mathrm{H}} m_{\mathrm{H}} + n_{\mathrm{He}} m_{\mathrm{He}}$. Replacing r with $N_{\mathrm{H}}/(\mu n_e)$ and plugging in relevant values,

$$M_{\mathrm{tot}} = 9.9 \times 10^{12}\ M_{\odot}\left(10^{-3([\mathrm{O/H}]+1)}\right)\left(\frac{n_e}{10^{-4}\ \mathrm{cm}^{-3}}\right)^{-2} f. \quad (3)$$

This is several times larger than estimates of the total Local Group binding mass, e.g., $M_{\mathrm{tot}} = (2.3 \pm 0.6) \times 10^{12}\ M_{\odot}$ as calculated by Courteau & van den Bergh (1999). Baryonic matter should only contribute $\sim$15% of this mass (if the baryon–to–dark matter ratio is equal to the cosmological value), so our estimate appears high. This discrepancy can be easily resolved with different values of [O/H] and f. For instance, if we assume an oxygen abundance of 0.3 times solar rather than 0.1, then the range of possible masses becomes $2.0 \times 10^{11} f\ M_{\odot} \leq M_{\mathrm{tot}} \leq 7.9 \times 10^{12} f\ M_{\odot}$. Thus, unless [O/H] is very high or $f \ll 1$, the O VII absorber almost certainly accounts for a major fraction of the baryonic matter in the Local Group. This sight line may also be probing gas that is not gravitationally bound to the Local Group (i.e., the Local filament), which may explain why our range of M_{tot} extends to such high values. Although Collins et al. (2005) argue that a Local Group origin requires that the O VII absorbers contain too much mass, we see here that the total mass is in fact consistent with expectations.

If this absorption does only trace the Local Group medium, then constraints on the extent of the absorber can be derived by assuming $M_{\mathrm{tot}} = 0.15 M_{\mathrm{LG}} \approx 3.5 \times 10^{11}\ M_{\odot}$. In this case, $r^3 f = 3M_{\mathrm{tot}}/[(4\pi)1.4\mu n_e m_{\mathrm{H}}]$. Taking the 2 σ upper limit of $\log n_{\mathrm{H}} = -3.9$, the 2 σ lower limit on $M_{\mathrm{LG}} = 1.1 \times 10^{12}\ M_{\odot}$, and assuming $f = 1$, we obtain a lower limit of $r > 0.2$ Mpc for the O VII absorption. Similarly, the upper limit on the radius is $r < 0.6 f^{-1/3}$ Mpc. This seems somewhat small compared to the actual size of the Local Group, but once again it is dependent on the geometry of the absorber. A value of $f \sim 0.1$ brings this upper limit more in line with the megaparsec scales expected in the Local Group; this may indicate that the Mrk 421 line of sight probes an extended, filamentary WHIM distribution. This calculation also assumes that the density of the Local Group medium is constant with radius, when the actual density profile is more likely centrally concentrated. These measurements are also affected by the O VI discrepancy: in case *b*, only the lower density limit of $\log n_e > -4.7$ (from the 2 σ O VI Kα upper limit) applies, so the upper radius and mass limits are still valid. Nevertheless, the consistency with the expected Local Group parameters is intriguing.

5.3. *Comparisons to Other Studies*

Kravtsov et al. (2002) used constrained simulations to study the properties of the Local Supercluster region; sky maps produced from this simulation (their Fig. 5) show filamentary structures near the Mrk 421 direction, possibly corresponding to the observed absorption. In addition, they note that a Local Group medium would exhibit a low Doppler parameter ($b \lesssim 60$ km s^{-1}) out to distances of $\sim$7 Mpc, consistent with our O VII measurement.

The inferred properties of the X-ray absorption along this line of sight also appear similar to other observations: toward 3C 273, for example, Fang et al. (2003) find $5.36 < \log T < 6.08$ and comparable O VII column density; however, their inferred O VII Doppler parameter is significantly higher than that toward Mrk 421: $b > 100$ km s^{-1}. On the other hand, the $z = 0$ absorber toward PKS 2155−304 (Nicastro et al. 2002) exhibits a temperature consistent with the Mrk 421 absorber, yet inferred density about an order of magnitude lower. Compared to the two intervening filaments seen toward Mrk 421 (Nicastro et al. 2005b), the density of the $z = 0$ absorption agrees with the derived lower limits ($\log n_e \gtrsim -5$ for both filaments), but the filaments appear to exhibit higher temperatures than that derived for the local absorption. These variations along different lines of sight simply demonstrate the complex nature of the absorption and the diversity of temperature and density environments produced in the structure formation process (e.g., Kravtsov et al. 2002).

The detection of X-ray absorption lines toward the Large Magellanic Cloud binary LMC X-3 by Wang et al. (2005) presents an important consideration for these results as well. The measured O VII and Ne IX equivalent widths and upper limits on O VIII and O VII$_{\mathrm{K}\beta}$ are all consistent with the same lines measured toward Mrk 421 (albeit with much larger statistical errors). Although this detection provides evidence of a hot intervening absorber between the Galaxy and LMC, it certainly does not rule out a primarily extragalactic origin for the Mrk 421 absorber. Any absorption, either Galactic or extragalactic, is likely to be inhomogeneous; thus, it is entirely plausible that the LMC X-3 sight line probes hot Galactic gas (perhaps enhanced by winds or outflows from both the Galaxy and LMC), while the absorption toward Mrk 421 is primarily due to low-density nearby WHIM gas.

6. SUMMARY AND FUTURE WORK

Through long-duration *Chandra* and *FUSE* observations of Mrk 421 in outburst, we have obtained unprecedented measurements of a variety of $z \sim 0$ absorption lines, many of which likely arise in extragalactic, partially photoionized gas. A brief summary of our results follows:

1. The relative strengths of the three O VII K series lines imply 2 σ Doppler parameter constraints of 24 km s^{-1} $< b <$ 55 km s^{-1}. This is inconsistent with the value of $b = 80.6 \pm 4.2$ km s^{-1} derived for the Galactic low-velocity O VI, indicating that the O VI$_{\rm LV}$ and O VII likely arise in different phases. The O VII b-value is, however, consistent with the local IGM simulations of Kravtsov et al. (2002) out to distances of several megaparsecs.

2. A weak high-velocity O VI λ1032 component also appears in the *FUSE* spectrum. Although its width is consistent with the O VII b measurement, the O VI$_{\rm HVC}$ column density is too low to be associated with the O VII absorption unless $T \gtrsim 10^7$ K (which itself is ruled out by the upper limit on b). The O VI$_{\rm HVC}$ may thus represent a distinct third component along this line of sight.

3. The column density inferred from the O VI Kα line is a factor of $\sim$4 higher than that measured from the O VI λ1032 transition. This may be due to unaccounted-for atomic physics effects, in which case the Kα line may provide a more accurate measurement of $N_{\rm O\ VI}$ than the λ1032 line. We consider both cases:

   (*a*) If the O VI Kα line measures $N_{\rm O\ VI}$, then strong constraints on the temperature, density, and relative abundances of the X-ray absorber can be derived: $T = 10^{5.5}$–$10^{5.7}$ K and $n_e = 10^{-4.7}$ to $10^{-3.9}$ cm^{-3}, with allowed abundances of $0.6 \leq [{\rm Ne/O}] \leq 2.2$, $-0.8 \leq [{\rm C/O}] \leq 0.3$, and $[{\rm N/O}] \leq 0.9$ (all 2 σ ranges). This range of densities, combined with $N_{\rm O\ VII}$, implies a total mass and extent consistent with those expected in the Local Group and/or Local filament if the gas metallicity is low. However, in this case the O VI UV–X-ray discrepancy becomes worse since (due to the Doppler parameter constraints) only a small portion of the O VI$_{\rm LV}$ line can be associated with the extragalactic X-ray lines.

   (*b*) If, instead, the O VI Kα line does not correctly measure $N_{\rm O\ VI}$, then the O VI associated with the O VII absorption must be fully blended with the Galactic O VI λ1032 and thus not measurable. In this case a lower density limit of $\log n_e > -4.7$ is found, which is consistent with either a Galactic or extragalactic medium.

Much work remains to be done, in order to both better understand the data presented here and determine the true nature of the $z \sim 0$ X-ray absorption. Higher S/N data along the Mrk 421 sight line would be useful to obtain better column density constraints, particularly on O VIII, O VI$_{\rm K\alpha}$, and Ne IX, and thus better constrain the effects of photoionization on the absorber. Data of comparable quality along other sight lines would be invaluable as well, both to probe other regions surrounding the Galaxy and to reconfirm the tantalizing O VI results presented herein. Higher resolution simulations of the Local Group may allow us to determine the ionic column densities expected in the WHIM and thus whether or not the observed absorption can possibly arise in the WHIM. Finally, more detailed modeling of O VI inner-shell transitions would shed a great deal of light on whether or not the O VI X-ray/UV discrepancy is real and thus provide an invaluable framework for studying new (and existing) X-ray data.

We thank the *Chandra* and *FUSE* teams for superb missions and the anonymous referee for helpful suggestions during the review process. R. J. Williams is supported by NASA through *Chandra* award AR5-6017X, F. Nicastro through *Chandra* grant GO3-4152X (fund 16617317) and 5 year LTSA grant NNG04GD49G, and T. Fang through *Chandra* Postdoctoral Fellowship Award PF3-40030. *Chandra* awards are issued by the *Chandra X-Ray Observatory* Center, which is operated by the Smithsonian Astrophysical Observatory for and on behalf of NASA under contract NAS8-39073. This work is based on observations made with the NASA-CNES-CSA *Far Ultraviolet Spectroscopic Explorer*. *FUSE* is operated for NASA by Johns Hopkins University under NASA contract NAS5-32985.

REFERENCES

Arav, N., Kaastra, J., Steenbrugge, K., Brinkman, B., Edelson, R., Korista, K. T., & de Kool, M. 2003, ApJ, 590, 174
Bennett, C. L., et al. 2003, ApJS, 148, 1
Cen, R., & Ostriker, J. P. 1999, ApJ, 514, 1
Chen, X., Weinberg, D. H., Katz, N., & Davé, R. 2003, ApJ, 594, 42
Collins, J. A., Shull, J. M., & Giroux, M. L. 2005, ApJ, 623, 196
Courteau, S., & van den Bergh, S. 1999, AJ, 118, 337
Danforth, C. W., Howk, J. C., Fullerton, A. W., Blair, W. P., & Sembach, K. R. 2002, ApJS, 139, 81
Danforth, C. W., & Shull, J. M. 2005, ApJ, 624, 555
Davé, R., et al. 2001, ApJ, 552, 473
Dickey, J. M., & Lockman, F. J. 1990, ARA&A, 28, 215
Drake, J., & Testa, P. 2005, Nature, 436, 525
Elvis, M., Marengo, M., & Karovska, M. 2002, ApJ, 567, L107
Fang, T., Marshall, H. L., Lee, J. C., Davis, D. S., & Canizares, C. R. 2002, ApJ, 572, L127
Fang, T., Sembach, K. R., & Canizares, C. R. 2003, ApJ, 586, L49
Ferland, G. J., 1996, Hazy: A Brief Introduction to CLOUDY 90, Univ. Kentucky, Phys. Dept. Internal Rep.
Garmire, G. P., Bautz, M. W., Ford, P. G., Nousek, J. A., & Ricker, G. R. 2003, Proc. SPIE, 4851, 28
Grevesse, N., & Anders, E. 1989, in AIP Conf. Proc. 183, Cosmic Abundances of Matter, ed. C. J. Waddington (New York: AIP), 1
Hellsten, U., Gnedin, N. Y., & Miralda-Escudé, J. 1998, ApJ, 509, 56
Howk, J. C., Sembach, K. R., & Savage, B. D. 2003, ApJ, 586, 249
Kravtsov, A. V., Klypin, A., & Hoffman, Y. 2002, ApJ, 571, 563
Krongold, Y., Nicastro, F., Brickhouse, N. S., Elvis, M., Liedahl, D. A., & Mathur, S. 2003, ApJ, 597, 832
Margon, B., Jones, T. W., & Wardle, J. F. C. 1978, AJ, 83, 1021
Marshall, H. L., Tennant, A., Grant, C. E., Hitchcock, A. P., O'Dell, S. L. & Plucinsky, P. P. 2004, Proc. SPIE, 5165, 497
Mathur, S., Weinberg, D. H., & Chen, X. 2003, ApJ, 582, 82
Murphy, E. M., Lockman, F. J., Laor, A., & Elvis, M. 1996, ApJS, 105, 369
Murray, S. S., & Chappell, J. H. 1986, Proc. SPIE, 597, 274
Nicastro, F., Elvis, M., Fiore, F., & Mathur, S. 2005a, in Clusters of Galaxies: New Insights from *XMM-Newton*, *Chandra*, and *INTEGRAL*, ed. J. Kaastra, in press (astro-ph/0501126)
Nicastro, F., et al. 2002, ApJ, 573, 157
———. 2003, Nature, 421, 719
———. 2005b, ApJ, 629, 700
———. 2005c, Nature, 433, 495
Paerels, F., et al. 2001, ApJ, 546, 338
Penton, S. V., Stocke, J. T., & Shull, J. M. 2000, ApJS, 130, 121
Perna, R., & Loeb, A. 1998, ApJ, 503, L135
Pradhan, A. K. 2000, ApJ, 545, L165
Pradhan, A. K., Chen, G. X., Delahaye, F., Nahar, S. N., & Oelgoetz, J. 2003, MNRAS, 341, 1268
Rasmussen, A., Kahn, S. M., & Paerels, F. 2003, in The IGM/Galaxy Connection: The Distribution of Baryons at z=0, ed. J. L. Rosenberg & M. E. Putman (ASSL Conf. Proc. 281; Dordrecht: Kluwer), 109
Savage, B. D., et al. 2003, ApJS, 146, 125
Schmidt, M., Beiersdorfer, P., Chen, H., Thorn, D. B., Träbert, E., & Behar, E. 2004, ApJ, 604, 562
Sembach, K. R. 2003, preprint (astro-ph/0311089)
Sembach, K. R., et al. 2003, ApJS, 146, 165
Shull, J. M., Stocke, J. T., & Penton, S. 1996, AJ, 111, 72

Sternberg, A., McKee, C. F., & Wolfire, M. G. 2002, ApJS, 143, 419
Verner, D. A., Verner, E. M., & Ferland, G. J. 1996, At. Data Nucl. Data Tables, 64, 1
Wakker, B. P., et al. 2003, ApJS, 146, 1
Wang, Q. D., et al. 2005, ApJ, submitted
Weinberg, D. H., Miralda-Escudé, J., Hernquist, L., & Katz, N. 1997, ApJ, 490, 564
Whittet, D. C. B. 1992, Dust in the Galactic Environment (Bristol: IOP)
Zsargó, J., Sembach, K. R., Howk, J. C., & Savage, B. D. 2003, ApJ, 586, 1019